Performance of an integrated multimodality image guidance and dose-planning system supporting tumor-targeted HDR brachytherapy for prostate cancer

Article *in* Radiotherapy and Oncology · November 2021

DOI: 10.1016/j.radonc.2021.11.026

CITATIONS
0

READS
23

14 authors, including:

David Grajales
Polytechnique Montréal
5 PUBLICATIONS **5** CITATIONS
SEE PROFILE

Samuel Kadoury
Polytechnique Montréal
204 PUBLICATIONS **4,586** CITATIONS
SEE PROFILE

Roozbeh Shams
Polytechnique Montréal
11 PUBLICATIONS **55** CITATIONS
SEE PROFILE

Guila Delouya
CHUM-Hopital Notre-Dame
144 PUBLICATIONS **917** CITATIONS
SEE PROFILE

Radiotherapy and Oncology 166 (2022) 154–161

Contents lists available at ScienceDirect

Radiotherapy and Oncology

journal homepage: www.thegreenjournal.com

Original Article

Performance of an integrated multimodality image guidance and dose-planning system supporting tumor-targeted HDR brachytherapy for prostate cancer

David Grajales [a,b], Samuel Kadoury [a,b], Roozbeh Shams [a], Maroie Barkati [b,c], Guila Delouya [b,c], Dominic Béliveau-Nadeau [b], Benedicte Nicolas [b], William Trung Le [a], Mustafa-Karim Benhacene-Boudam [b], Daniel Juneau [b,c], Jean N. DaSilva [b,c], Jean-Francois Carrier [b,c], Gilion Hautvast [d], Cynthia Ménard [b,c,*]

[a] Polytechnique Montréal; [b] Centre de Recherche du Centre Hospitalier de l'Université de Montréal, Canada; [c] Université de Montréal, Canada; [d] Philips Healthcare, Imaging Systems, Netherlands

ARTICLE INFO

Article history:
Received 21 July 2021
Received in revised form 19 November 2021
Accepted 22 November 2021
Available online 30 November 2021

Keywords:
Prostate cancer
Brachytherapy
Image registration
Electromagnetic tracking
Navigation system

ABSTRACT

Background and purpose: Advances in high-dose-rate brachytherapy to treat prostate cancer hinge on improved accuracy in navigation and targeting while optimizing a streamlined workflow. Multimodal image registration and electromagnetic (EM) tracking are two technologies integrated into a prototype system in the early phase of clinical evaluation. We aim to report on the system's accuracy and workflow performance in support of tumor-targeted procedures.

Materials and methods: In a prospective study, we evaluated the system in 43 consecutive procedures after clinical deployment. We measured workflow efficiency and EM catheter reconstruction accuracy. We also evaluated the system's MRI-TRUS registration accuracy with/without deformation, and with/without y-axis rotation for urethral alignment at initialization.

Results: The cohort included 32 focal brachytherapy and 11 integrated boost whole-gland implants. Mean procedure time excluding dose delivery was 38 min (range: 21–83) for focal, and 56 min (range: 38–89) for whole-gland implants; stable over time. EM catheter reconstructions achieved a mean difference between computed and measured free-length of 0.8 mm (SD 0.8, no corrections performed), and mean axial manual corrections 1.3 mm (SD 0.7). EM also enabled the clinical use of a non or partially visible catheter in 21% of procedures. Registration accuracy improved with y-axis rotation for urethral alignment at initialization and with the elastic registration (mTRE 3.42 mm, SD 1.49).

Conclusion: The system supported tumor-targeting and was implemented with no demonstrable learning curve. EM reconstruction errors were small, correctable, and improved with calibration and control of external distortion sources; increasing confidence in the use of partially visible catheters. Image registration errors remained despite rotational alignment and deformation, and should be carefully considered.

High-dose-rate (HDR) brachytherapy is an established treatment modality for localized prostate cancer (PCa), the most common cancer in men in North America (excluding non-melanoma skin cancer) with more than 235,000 new cases in 2020 [1,2]. By virtue of underlying physics, the safety and effectiveness of this modality hinge on accurate targeting [3]. Transrectal ultrasound (TRUS) is commonly used to guide brachytherapy, biopsies, and other prostate interventions due to its real-time nature, ease of use, and low cost [4]; nevertheless, most cancers are invisible in TRUS [4–6]. On the other hand, multiparametric MRI and prostate-specific membrane antigen (PSMA)-PET/CT have greater sensitivity and specificity (respectively) for the localized characterization of PCa [4,7–9]. However, these are not optimal modalities to guide interventions due to longer acquisition time, limited compatibility with surgical instruments, and cost [1,4].

Multimodal image registration is currently studied and used to take advantage of complementary information to assist HDR brachytherapy and other tumor-targeted prostate interventions. Some of these interventional systems, such as BiopSee (Pi Medical), PredictiveFusion (MIM software) and SmartFusion (Canon medical

* Corresponding author at: Département de radio-oncologie, Centre Hospitalier de l'Université de Montréal (CHUM), 1051 rue Sanguinet, Montréal, Québec H2X 0C1, Canada.
E-mail address: cynthia.menard@umontreal.ca (C. Ménard).

https://doi.org/10.1016/j.radonc.2021.11.026
0167-8140/

Systems), work by rigidly fusing preoperative MRI with intraoperative TRUS [8,10–12]. However, rigid registration accuracy is not ideal due to gland deformation caused by an altered patient position, TRUS-probe placement, or brachytherapy catheter insertion; these accumulated uncertainties can lead to target registration errors over 5 mm [4,11]. To compensate for these variations, several elastic registration methods have been developed based on target landmarks, organ surfaces, and image intensity [4,12–15]. Fusion systems like Artemis (Eigen) and Urostation (Koelis) are already used to guide prostate biopsies, applying multimodal elastic image registration [8,16,17].

In HDR brachytherapy workflow, the accurate placement and localization of catheters are as important as the localization of treatment targets. Current TRUS-guided systems allow manual catheter reconstruction where depth is inferred from measured catheter free-lengths (defined as the section of the known-length catheters extending from the template), which is a time-consuming process; when multiple catheters are in place, interference could affect localization accuracy, significantly impacting dose delivery and treatment outcomes [18,19]. Electromagnetic (EM) tracking is a technology used during minimally invasive interventions for catheter localization and reconstruction [19,20]. The EM system consists of a field generator, a set of coils or sensors tracked within the generator's region of influence, and a control unit that processes sensors' signals to determine their location and orientation. The catheter reconstruction is done by introducing an EM tracked stylus into each catheter [18,20,21].

Given the complexity required to achieve high precision and accuracy during HDR brachytherapy procedures, systems that integrate all steps in a streamlined workflow are needed. In this study, we evaluate the performance of a prototype navigation system for HDR brachytherapy, which is in the early phase of clinical deployment. Our analysis of workflow performance, registration, and catheter reconstruction accuracy intends to determine the potential of a system that combines multimodal elastic image registration with EM tracking for HDR brachytherapy guidance.

Methods and materials

Clinical data and equipment

Between September 2019 and December 2020, 34 patients with histological diagnosis of PCa were enrolled on a prospective clinical trial approved by the Research Ethics Board (NCT03378856), and underwent HDR brachytherapy using the prototype system. Nine of these patients underwent two separate interventions. In total, 43 procedures were included in the analysis of the system's performance.

Prior to the procedure, a planning MRI (3D T2-weighted FSE, b2000 DWI, +/− DCE) was obtained on a 1.5T Siemens Aera Magnetom (Siemens Healthineers, Erlangen, Germany) using surface coils. PSMA-PET/CT (^{18}F-DFCPyL [22]) images were also acquired in a subset. For intraoperative imaging, two different ultrasound systems were used: BK Flex-Focus and bk3000 using a BK endocavity biplane transducer (BK Ultrasound, Herlev, Denmark).

The prototype system (Invivo/UroNav, Philips Disease Management Solutions, Gainesville, USA) was designed to support prostate tumor-targeting with the integration of multimodal image registration, while improving procedural workflow efficiencies and catheter reconstruction accuracy through EM tracking. The integrated EM system (Aurora NDI, Waterloo, Canada) consists of an EM field generator placed over the patient's pelvic region, EM sensors placed on the template and TRUS-probe holder, and an EM stylus to reconstruct the catheters (Fig. 1).

For accurate EM tracking, the system was calibrated twice: before the first case (calibration 1: including template and TRUS-probe sensors) and before intervention number 27 (calibration 2: including template and TRUS-probe sensors, this time with the metallic leg holders and revised probe holder in place) due to observed systematic shifts. The EM systems could be susceptible to distorting equipment present in the operation room, including cellphones. For the last 6 cases, the radiation oncologist (RO) performing the procedure was instructed not to carry a cellphone, removing a potential source of error.

Fig. 1. Clinical setup: A) prototype navigation and dose-planning system, B) ultrasound system, C) EM field generator-tracking system.

Workflow

Pre-procedure: Planning images (MRI and PET) were co-registered for precise tumor localization, and manual segmentation of the prostate, GTV, PTV, and visible urethra was performed by the RO (Eclipse, Varian Medical Systems, Palo Alto, USA). T2-weighted images and corresponding segmentations were then transferred to the prototype system.

Intra-procedure: After set-up in the brachytherapy suite, baseline interventional 3D-TRUS images were reconstructed through manual sagittal sweep, followed by manual segmentation of the prostate and urethra/indwelling foley catheter. MRI and TRUS images and contours were first initialized with rigid registration based on prostate segmentations' center of mass (COM) and manual y-axis rotation (around right-left axis) for urethral alignment. Using the contour-based algorithm of the prototype system, deformable registration was then performed, enabling visualization of deformed structures projected over real-time TRUS within the navigation system. Manual segmentation of GTV and PTV on TRUS images was then performed based on these projections (propagated MRI contours) and underlying TRUS contrast. A preplan was generated based on a predefined prescription template, and proposed catheter sites were displayed.

Catheter implantation proceeded with attempts to maintain visibility on TRUS, and a final 3D-TRUS volume was acquired for treatment planning. The EM stylus was fully inserted in each catheter then slowly retracted to create a 3D reconstruction of dwell paths; the reconstruction was manually adjusted (in the axial plane) to align with the visible catheter in the TRUS images.

Catheter depths were then verified against measured free-lengths. Segmented structures (TRUS prostate segmentation and the segmentations anchored to it) were subsequently adjusted as needed based on prostate displacements incurred with needle insertion, and a final treatment plan was generated with an inverse planning algorithm. All data (images, segmentations, transformation matrices, RT plan) were stored locally.

Performance evaluation

The open-source 3D-Slicer platform [23], version 4.11.0-2020-02-12, was used to visualize and process DICOM RTData. The system's evaluation focused on three aspects: workflow performance, catheter reconstruction accuracy, and elastic registration accuracy.

Related to workflow efficiency, we evaluated the duration of the intervention, calculated between the first 3D-TRUS acquisition and the last approved RTPlan. For catheter reconstruction accuracy, the measured free-length was compared to computed free-length as a measure of depth accuracy; and the distance between catheter reconstruction corresponding points (considering only catheters' segment inside the prostate) before and after the manual adjustments.

For registration accuracy, MRI segmentations were rigidly registered to the TRUS volume using the initialization transformation matrix used and stored during the procedure, including the manual rotation when applied. The elastic deformation field was retrospectively calculated based on MRI and TRUS prostate surface contours, using the prototype system's algorithm. This deformation field was then applied to the MRI segmentations.

The following metrics were calculated before and after deformation to assess the rigid and deformable (elastic) registration accuracy:

Target Registration Error (TRE): Up to 5 landmarks (e.g., cyst, calcification) were screened and selected by an expert RO on both TRUS and MRI. The distances between the corresponding landmarks were calculated and compared using the SlicerRegistrationQA module. The mean TRE (mTRE) was then calculated for all the cases.

Urethral midline – 3D distance: Two sets of points (range: 16–25) were placed on the midline of MRI and TRUS urethra segmentation (in the center of equidistant cross-section). The MRI points were used to create a 3D model of the MRI urethral midline. The distances between the TRUS set of points and the closest point in the MRI urethral midline model were calculated and compared. This process was made using the SlicerCurveMaker extension.

Dice Similarity Coefficient (DSC) and 95%-Hausdorff distance: These two similarity metrics were used to verify that the surface-based deformation was working properly. They were calculated using the SlicerSegmentComparison module.

Impact of initialization procedures

In this application, the initialization point for the elastic registration is the position of the prostate segmentation in both modalities before starting the elastic deformation. Three different initializations were evaluated:

Centered: The volumes were centered using a translation based on the COM of the prostate segmentation ROIs from both modalities.

Autoaligned: The volumes were automatically aligned based on the urethral segmentation. In this method, the superior and inferior urethral points (center of urethra cross-section at the intersection of the prostate boundary) were connected by a line in both modalities. Then, the MRI volume was rotated, such that the lines would be oriented along a common axis. Finally, the MRI volume was translated to match the urethra inferior point (point of highest confidence) in both modalities.

Manual: After the COM translation applied by the system, the MRI volumes were rotated manually to align the urethra in y-axis, when the treating team considered it needed.

A 3D-Slicer extension (SegRegUrethra) was developed to calculate the transformation matrix for the centered and autoaligned initializations. For each initialization point, the deformation field was retrospectively calculated using the prototype system's algorithm. The same metrics described in the previous section were computed to compare the final effect of pre-alignment.

Statistical analysis

The differences were evaluated using a paired and two-samples Student's t-test (two-sided). A p-value <0.01 was considered as a statistically significant difference. Boxplots show the median (central mark), 25th–75th percentiles (box), extreme data not including outliers (whiskers) and outliers (+). Mean values are reported as mean (SD).

Results

Of the 43 cases, 32 consisted of focal brachytherapy implants, and 11 consisted of integrated boost (IB) implants. After automatic centering, 29 cases were manually rotated about the y-axis to correct the alignment of the urethra in sagittal images (caused by rotation of the pelvis in lithotomy position) prior to deformable registration.

The procedure time is shown in Fig. 2.A. The mean duration was 43.1 min (range: 21.4–88.7); when discriminating by focal and IB, the duration was 38.6 min (range: 21.4–83.1) and 56.0 min (range: 37.5–88.7), respectively. A learning curve was not demonstrated.

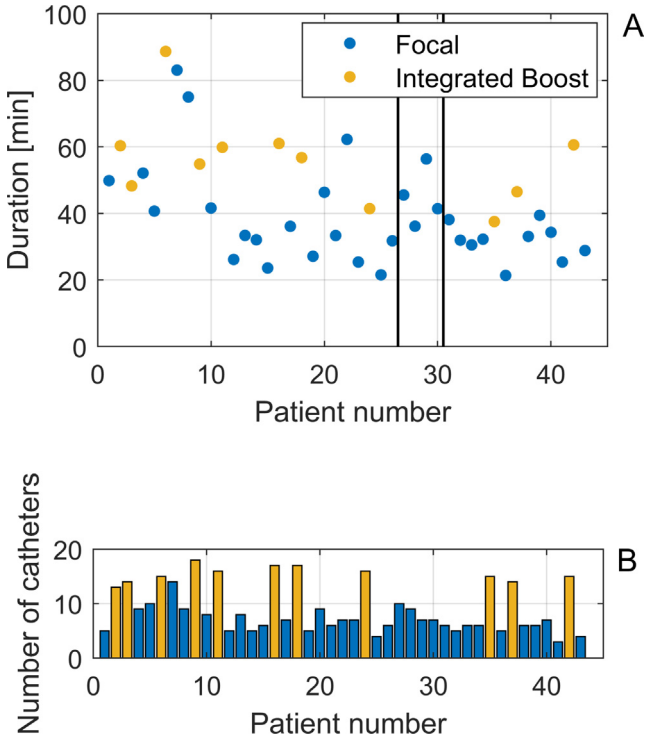

Fig. 2. A) Procedure duration and B) number of catheters for each intervention. The duration was calculated between the first 3D-TRUS reconstruction and the last approved RT plan. Each black line indicates a 3-month pause due to COVID-19.

In total, 387 catheters were implanted (Fig. 2.B). The mean number of catheters per case was 9 (range: 3–18); for IB procedures, the mean was 15 (range: 13–18), and for focal 7 (range: 3–14). In 21% of the procedures, at least one (range: 1–3) partially-visible catheter was enabled for use in treatment planning due to the added information provided by EM reconstruction, where the offset was minimal or systematic for all other visible catheter reconstructions in the implant (internal validation).

On the superior-inferior axis, computed and measured catheter free-lengths presented a submillimeter systematic offset with a mean of 0.85(0.81) mm.

In the axial view, 64% of EM catheter reconstructions required millimetric manual in-plane adjustments, based on visible catheters in TRUS (Fig. 3.A). The 3D distances between corresponding points in the original and adjusted reconstruction were calculated to find each catheter's mean and maximum distance. These results can be divided into three subsets: after the first calibration of the system, after the second calibration, and after the second calibration but with the cell phone removed from the field, as shown in Table 1. The maximum applied manual adjustments are presented in Fig. 3.B.

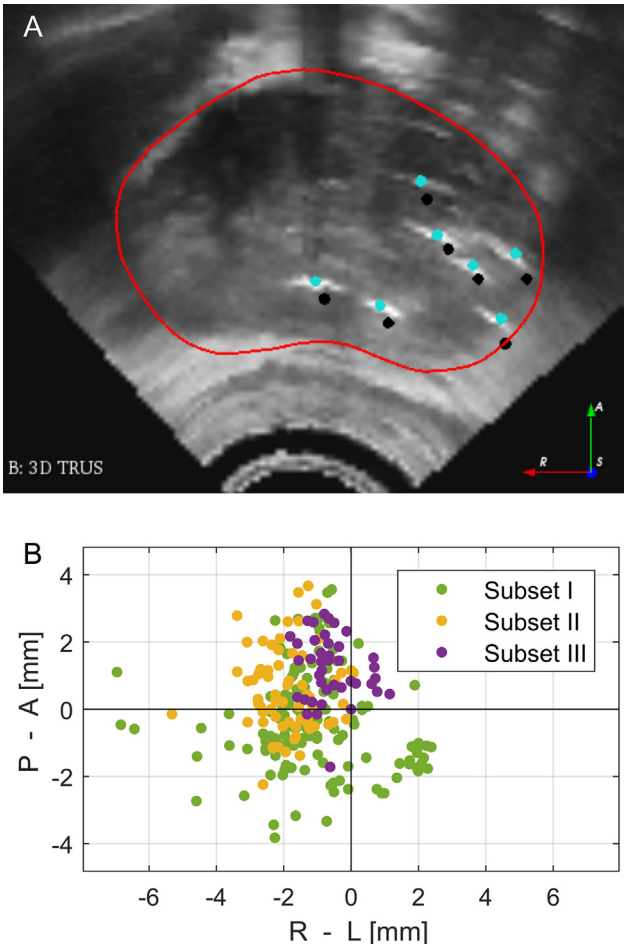

Fig. 3. A) Visualization of original (black) and adjusted (cyan) catheter reconstructions, and prostate segmentation (red) for a sample case, in axial view. B) Maximum applied manual adjustments per catheter based on 3D distance between corresponding points. The three subsets correspond to I) calibration 1 with external interference (256 catheters), II) calibration 2 with external interference (90 catheters), and III) calibration 2 without external interference (41 catheters). (For interpretation of the references to colour in this figure legend, the reader is referred to the web version of this article.)

Comparing subsets I and II, no significant difference was found for mean distance (p = 0.415) nor maximum distance (p = 0.762). The differences between subsets II and III were significant for both mean distance (p = 2.6E-7) and maximum distance (p = 0.002). As shown in Fig. 3.B and by P95% on Table1, the distance of extreme cases decreased from I to II, and even more for III.

The calculated metrics for elastic registration accuracy are presented in Fig. 4, with the corresponding p-value.

Six cases were excluded (0 landmarks identified) from the TRE analysis. Nine cases had 1 landmark, 15 cases had 2 landmarks, 8 cases had 3 landmarks, 8 cases had 4 landmarks, and only 1 case had 5 landmarks. Of the 37 evaluated cases (Fig. 4.A), the mTRE was 3.98(1.99) mm after rigid and before elastic registration. After applying the elastic registration, the mTRE was 3.41(1.48) mm.

To compare urethral midline distance (Fig. 4.B), 2 cases were excluded due to poor visibility of the urethra on MRI, which did not allow reliable segmentation. The mean distance before and after deformation was 3.26(1.99) mm and 2.89(1.24) mm, respectively.

Prostate contours agreement was observed after deformation as expected given the use of a surface-based elastic registration algorithm (Fig. 4.C-D). Mean DSC was 0.82(0.08) and 0.94(0.02) after rigid and after elastic registration, respectively. The mean 95%-Hausdorff distance was 5.08(1.96) mm before deformation and 1.92(0.73) mm after deformation.

Fig. 5 illustrates an example of the three initialization points. Since the proposed method for automatic alignment is based on urethral segmentations, 2 cases were excluded from this analysis (all metrics) due to the lack of urethra segmentation on MRI. Four more cases were excluded from mTRE assessment (0 landmarks identified). Fig. 6 presents the results for the three initializations and the p-values comparing the autoaligned method to the others.

The mTRE after deformation was 4.39(2.03) mm for the autoaligned initialization and 4.57(2.13) mm for centered volumes (Fig. 6.A). For the manual initialization point (the one used during the intervention), the mTRE was 3.42(1.49) mm, but the difference was not significant (p > 0.01).

The mean distance between urethral midlines of 2.16(0.89) mm for the autoaligned initialization (Fig. 6.B) was statistically smaller than both centered at 3.25(1.16) mm and manual at 2.89(1.24) mm.

Finally, the mean 95%-Hausdorff distance was 1.73(0.55) mm for centered, 2.01(0.81) mm for autoaligned, and 1.93(0.75) mm for manual initialization; mean DSC was 0.94(0.02) for the 3 initializations. No significant difference was found for both metrics (Fig. 6.C-D).

Discussion

In this study, we evaluated the clinical performance of a prototype system for HDR brachytherapy with regards to workflow efficiencies, EM catheter reconstruction accuracy, and multimodality image registration accuracy.

Average procedure time for conventional (no EM tracked) TRUS-guided prostate HDR brachytherapy is reported from 85 to 120 min, including 15 to 20 min of set-up [18,24,25]. The procedure workflow for the prototype system compared favorably with current standard-of-care practice and was integrated with little, if any, learning curve as observed in our timeline of procedural efficiencies.

In traditional non-tracking systems, catheter reconstruction is based on the image signature and measures of catheter free-length. This can be challenging due to inherent artifacts of images, especially in the context of implanted devices [26]. In focal salvage treatments, the high number of catheters in a small volume (pres-

Table 1
3D distances between corresponding points in the original and adjusted catheter reconstructions in the prostate region. "$P_{95\%}$" represents the 95 percentile of the data, and "-" denotes the cases where the radiation oncologist was not carrying a cellphone.

Subset	External interference	Calibration	No. Catheters	Mean Distance [mm]		Maximum Distance [mm]	
				Mean (SD)	$P_{95\%}$	Mean (SD)	$P_{95\%}$
I	+	1	256	1.95 (1.22)	3.90	2.29 (1.40)	4.37
II	+	2	90	2.06 (1.09)	3.29	2.24 (1.23)	3.79
III	-	2	41	**1.26 (0.65)**	**2.22**	**1.69 (0.71)**	**2.87**
All cases			387	1.87 (1.17)	3.41	2.18 (1.33)	3.82

ence of shadowing or strong reflection) can exacerbate this problem, such that some catheters only be partially visible on TRUS [1,26,27]. EM tracking can increase confidence in catheter reconstruction (especially in depth). The residual error in free-length is less than the tolerance for non-tracking systems with high-quality images (1 mm) [28]. As demonstrated in 9 procedures, EM tracking also increases confidence in use of partially visible catheters in an otherwise accurately reconstructed implant. However based on our results, the use of EM tracking alone without global image validation is not recommended.

Flexible catheters can be bent by anterior pressure from the TRUS-probe. Given that the EM reconstruction is made using a rigid stylus, we observe a systematic anterior-posterior displacement, more pronounced at the distal tip [21,26]. Seventy-two % of manual adjustments were smaller than 2 mm, which is the reported tolerance for non-tracking systems [28], and 95% were smaller than 3 mm, which is a displacement reported to impact dose plans [29]. Nonetheless, we recognized that such errors could be clinically significant thereby motivating calibration 2. Calibration and control of external interference sources (cellphone) significantly improved the accuracy of catheter reconstruction, with remaining displacements due to catheter flexibility. Image-based corrections of EM reconstructions remain essential in this workflow. Other possible causes of interference (even distant to the EM field, e.g., US system) should be studied to identify possible causes of the remaining systematic right shift.

One of the challenges of multimodal image registration for prostate applications is the deformation of structures due to rotation of the pelvis, the presence of an endorectal probe, the placement of a foley catheter, and the insertion of brachytherapy catheters; hence the need to investigate elastic registration and to evaluate its performance in real conditions [4,11].

Surface-based elastic registration displayed slightly better results (mTRE) than rigid registration, but uncertainties remain. The mTRE value after deformation is within the reported range (2.1–3.7 mm) for similar systems [3,12,13]. Although mTRE is one of the most widely used metrics for assessing image registration performance [4], 1 or 2 landmarks in 56% of the cases make these results very localized and dependent on the specific location of the landmark (e.g., distance to the surface).

The urethra is an important reference structure in prostate interventions because of its visibility in different modalities. Besides, it is crucial to consider the urethra location during HDR brachytherapy to minimize radiation damage [1,3]. The distance

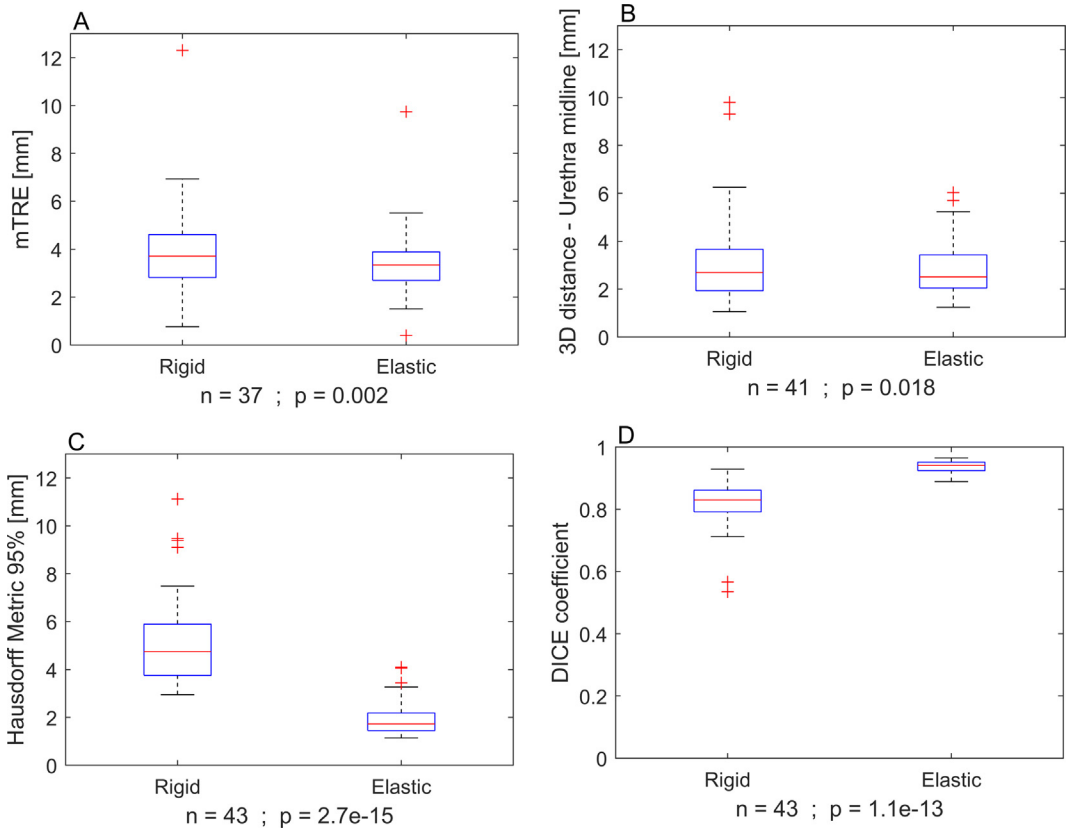

Fig. 4. Performance comparison for rigid and elastic registration methods. A) mTRE, B) Urethral midline 3D distance, C) 95%-Hausdorff, and D) DSC.

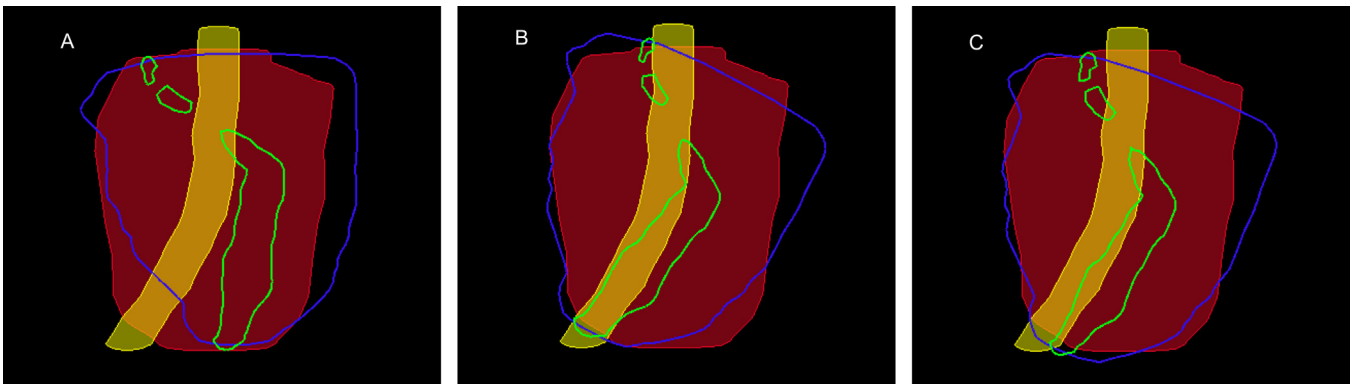

Fig. 5. Representation of A) centered, B) autoaligned, and C) manual initialization points for a sample case. Filled slices are from TRUS segmentation and contours from MRI segmentation: prostate (red and blue) and urethra (yellow and green). (For interpretation of the references to colour in this figure legend, the reader is referred to the web version of this article.)

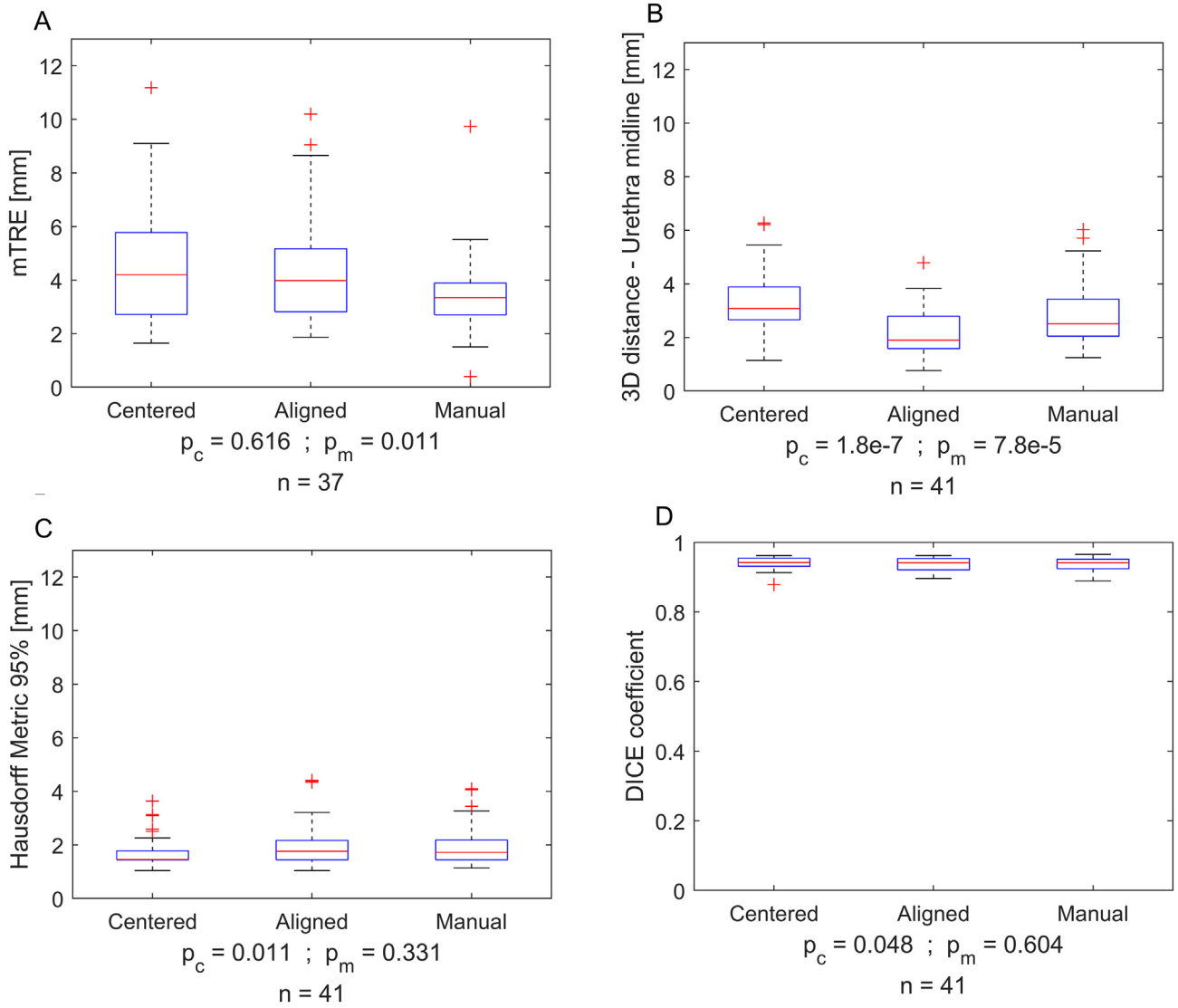

Fig. 6. Evaluation of the elastic registration method for three different initialization points; pc was used to compare autoaligned-centered start points and pm autoaligned-manual. A) mTRE, B) Urethral midline 3D distance, C) 95%-Hausdorff, and D) DSC.

between urethral midlines after deformation was reduced by 0.36 mm (not statistically significant), but the achieved distance is within the accuracy range reported for the system (2–3 mm) [13]. When using point-based metrics, the verification validity for the overall image registration improves by increasing the number of points [30]. Urethra visibility allowed the use of more points (range: 16–25) distributed along the gland, it provides a clearer depiction of the algorithm's performance in the prostate, within the central region. Since the urethra is easier to identify than landmarks, usage of more reference points reduced the impact of the error added by manual segmentation [31].

Cognitive or rigid computational registration, typically performed when physicians wish to use MRI information during the brachytherapy procedure, are known to carry errors. Although we demonstrate that important uncertainties remain with elastic registration, we were able to demonstrate that this strategy improves accuracy without compromising workflow performance [17,32].

It is well established that MRI and TRUS images are acquired at different pelvic rotations around the right-left axis. Such rotations can be large and lead to errors in registration if not corrected a priori; surface-based registration algorithms do not normally include automatic rotation in the basic workflow (additional segmentations or fiducial selection would be needed) but usually include tools to do it manually. We found that both an automated and a manual approach to align the urethral angle prior to applying deformable registration improved registration accuracy (33% and 11%, respectively) as measured by the urethral midline distance. As expected for a surface-based algorithm, Hausdorff and DSC did not show significant differences for the three initializations since the similarity of the contours is optimized during the elastic registration [4], showing that the initialization does not affect the performance of the algorithm on the surface. Finally, regarding mTRE, no significant results were obtained when comparing the manual initialization and our automated method at the specific sites of the landmarks.

In future work, we aim to further advance the technique to minimize requirements for manual catheter reconstruction adjustments (e.g., flexible EM tracked stylus), and to refine software tools for such manual adjustments. Furthermore, the integration of autosegmentation on TRUS (prostate, urethra, catheters) could greatly improve time efficiencies. Finally, attempts to better approach pre-planning geometry at set-up may further improve registration performance. Each step will contribute to our vision of a highly streamlined procedure that can be performed under 30 min with minimal anesthesia requirements, and with high accuracy and confidence. This vision can only be achieved with the full integration of a suite of technical innovations.

Conclusion

We found that workflow efficiency and technical performance of a prototype navigation system supporting tumor-targeted HDR prostate brachytherapy aligned with our current clinical practice and was not disruptive of our clinical throughput despite its added underlying complexity. EM tracking is accurate enough to complement catheter reconstruction combined with TRUS, and occasionally enabled the use of catheters that were clinically well-positioned within an accurately reconstructed implant, but that were partially visible in TRUS. Although gains were demonstrated with the system's deformable image registration tools compared with rigid alignment, uncertainties remain and must be considered when defining the PTV. Finally, an automated tool to align the urethral angle before applying deformable registration, as proposed in this evaluation, is justified.

Funding, sources of support and acknowledgements

- Funded in part with in kind support from Philips InVivo, and Grant awards from Varian Medical systems and NSERC/CIHR.
- This research was undertaken thanks, in part, to funding from the Canada First Research Excellence Fund through the TransMedTech Institute.

Conflict of interest statement

None.

References

[1] Dutta SW, Alonso CE, Libby B, Showalter TN. Prostate cancer high dose-rate brachytherapy: review of evidence and current perspectives. Expert Rev Med Devices 2018;15:71–9. https://doi.org/10.1080/17434440.2018.1419058.
[2] Sung H, Ferlay J, Siegel RL, Laversanne M, Soerjomataram I, Jemal A, et al. Global Cancer Statistics 2020: GLOBOCAN estimates of incidence and mortality worldwide for 36 cancers in 185 countries. CA Cancer J Clin 2021;71:209–49. https://doi.org/10.3322/caac.21660.
[3] Gomez-Iturriaga A, Crook J, Casquero F, Carvajal C, Urresola A, Canteli B, et al. Impact of intraoperative MRI/TRUS fusion on dosimetric parameters in cT3a prostate cancer patients treated with high-dose-rate real-time brachytherapy. J Contemp Brachytherapy 2014;2:154–60. https://doi.org/10.5114/jcb.2014.43299.
[4] Zhang Y, Bi J, Zhang W, Du H, Xu Y. Recent advances in registration methods for MRI-TRUS fusion image-guided interventions of prostate. Recent Patents Eng 2017;11:115–24. https://doi.org/10.2174/1872212110666161201115248.
[5] Yang T, Zhang L, Chen Y, Cai Y, Jiang H, Ding Q. The predictive efficacy of hypoechoic lesion in ultrasound for prostate cancer in Chinese people: five-year experience in a moderated 10-core transperineal prostate biopsy procedure. Oncotarget 2017;8:79433–40. https://doi.org/10.18632/oncotarget.18342.
[6] Kadoury S, Wood BJ, Venkatesan AM, Dalal S, Xu S, Kruecker J. Accuracy assessment of an automatic image-based PET/CT registration for ultrasound-guided biopsies and ablations. Med. Imaging 2011 Vis. Image-Guided Proced. Model., 7964, 2011, p. 818–26. https://doi.org/10.1117/12.878067.
[7] Bouchelouche K, Choyke PL. PSMA PET in prostate cancer – a step towards personalized medicine. Curr Opin Oncol 2016;28:216–21. https://doi.org/10.1097/CCO.0000000000000277.
[8] Venderink W, Bomers JG, Overduin CG, Padhani AR, de Lauw GR, Sedelaar MJ, et al. Multiparametric magnetic resonance imaging for the detection of clinically significant prostate cancer: what urologists need to know. Part 3: Targeted biopsy. Eur Urol 2020;77:481–90. https://doi.org/10.1016/j.eururo.2019.10.009.
[9] Blanchard P, Ménard C, Frank SJ. Clinical use of magnetic resonance imaging across the prostate brachytherapy workflow. Brachytherapy 2017;16:734–42. https://doi.org/10.1016/j.brachy.2016.11.012.
[10] Zogal P, Sakas G, Rösch W, Baltas D. BiopSee® - Transperineal stereotactic navigated prostate biopsy. J Contemp Brachytherapy 2011;3:91–5. https://doi.org/10.5114/jcb.2011.23203.
[11] van de Ven WJM, Venderink W, Sedelaar JPM, Veltman J, Barentsz JO, Fütterer JJ, et al. MR-targeted TRUS prostate biopsy using local reference augmentation: initial experience. Int Urol Nephrol 2016;48:1037–45. https://doi.org/10.1007/s11255-016-1283-2.
[12] Poulin E, Boudam K, Pinter C, Kadoury S, Lasso A, Fichtinger G, et al. Validation of MRI to TRUS registration for high-dose-rate prostate brachytherapy. Brachytherapy 2018;17:283–90. https://doi.org/10.1016/j.brachy.2017.11.018.
[13] Sparks R, Bloch BN, Feleppa E, Barratt D, Madabhushi A. Fully automated prostate magnetic resonance imaging and transrectal ultrasound fusion via a probabilistic registration metric. Med. Imaging 2013 Image-Guided Proced. Robot. Interv. Model., vol. 8671, 2013, p. 86710A. https://doi.org/10.1117/12.2007610.
[14] Kadoury S, Yan P, Xu S, Glossop N, Choyke P, Turkbey B, et al. Realtime TRUS/MRI fusion targeted-biopsy for prostate cancer: a clinical demonstration of increased positive biopsy rates. Prostate cancer imaging comput diagnosis. Progn Interv 2010;6367:52–62. https://doi.org/10.1007/978-3-642-15989-3_7.
[15] Hu Y, Ahmed HU, Allen C, Pendsé D, Sahu M, Emberton M, et al. MR to ultrasound image registration for guiding prostate biopsy and interventions. Med Image Comput Comput Interv – MICCAI 2009 2009;5761:787–94. https://doi.org/10.1007/978-3-642-04268-3_97.
[16] Streicher J, Lee Meyerson B, Karivedu V, Sidana A. A review of optimal prostate biopsy: indications and techniques. Ther Adv Urol 2019;11:1–8. https://doi.org/10.1177/1756287219870074.
[17] Logan JK, Rais-Bahrami S, Turkbey B, Gomella A, Amalou H, Choyke PL, et al. Current status of magnetic resonance imaging (MRI) and ultrasonography fusion software platforms for guidance of prostate biopsies. BJU Int 2014;114:641–52. https://doi.org/10.1111/bju.12593.

[18] Beaulieu L, Racine E, Han DY, Vigneault E, Hsu I-C, Cunha JAM. Real-time electromagnetic tracking–based treatment platform for high-dose-rate prostate brachytherapy: clinical workflows and end-to-end validation. Brachytherapy 2018;17:103–10. https://doi.org/10.1016/j.brachy.2017.04.247.
[19] Kirisits C, Rivard MJ, Baltas D, Ballester F, De Brabandere M, van der Laarse R, et al. Review of clinical brachytherapy uncertainties: analysis guidelines of GEC-ESTRO and the AAPM. Radiother Oncol 2014;110:199–212. https://doi.org/10.1016/j.radonc.2013.11.002.
[20] Franz AM, Haidegger T, Birkfellner W, Cleary K, Peters TM, Maier-Hein L. Electromagnetic tracking in medicine - a review of technology, validation, and applications. IEEE Trans Med Imaging 2014;33:1702–25. https://doi.org/10.1109/TMI.2014.2321777.
[21] Bharat S, Kung C, Dehghan E, Ravi A, Venugopal N, Bonillas A, et al. Electromagnetic tracking for catheter reconstruction in ultrasound-guided high-dose-rate brachytherapy of the prostate. Brachytherapy 2014;13:640–50. https://doi.org/10.1016/j.brachy.2014.05.012.
[22] Dornan MH, Simard JM, Leblond A, Juneau D, Delouya G, Saad F, et al. Simplified and robust one-step radiosynthesis of [18F]DCFPyL via direct radiofluorination and cartridge-based purification. J Label Compd Radiopharm 2018;61:757–63. https://doi.org/10.1002/jlcr.3632.
[23] Fedorov A, Beichel R, Kalpathy-Cramer J, Finet J, Fillion-Robin J-C, Pujol S, et al. 3D Slicer as an image computing platform for the Quantitative Imaging Network. Magn Reson Imaging 2012;30:1323–41. https://doi.org/10.1016/j.mri.2012.05.001.
[24] Banerjee S, Kataria T, Gupta D, Goyal S, Bisht SS, Basu T, et al. Use of ultrasound in image-guided high-dose-rate brachytherapy: enumerations and arguments. J Contemp Brachytherapy 2017;2:146–50. https://doi.org/10.5114/jcb.2017.67456.
[25] Zhang H, Kang S, Ali N, Baran A, Bylund K, Gentile D, et al. Building a high-dose-rate prostate brachytherapy program with real-time ultrasound-based planning: initial safety, quality, and outcome results. Adv Radiat Oncol 2020;5:388–95. https://doi.org/10.1016/j.adro.2020.02.002.
[26] Zhou J, Zamdborg L, Sebastian E. Review of advanced catheter technologies in radiation oncology brachytherapy procedures. Cancer Manag Res 2015;7:199–211. https://doi.org/10.2147/CMAR.S46042.
[27] Batchelar DL, Chung HT, Loblaw A, Law N, Cisecki T, Morton GC. Intraoperative ultrasound-based planning can effectively replace postoperative CT-based planning for high-dose-rate brachytherapy for prostate cancer. Brachytherapy 2016;15:399–405. https://doi.org/10.1016/j.brachy.2016.04.003.
[28] Smith BR, Strand SA, Dunkerley D, Flynn RT, Besemer AE, Kos JD, et al. Implementation of a real-time ultrasound-guided prostate HDR brachytherapy program. J Appl Clin Med Phys 2021;22:189–214. https://doi.org/10.1002/acm2.13363.
[29] Kolkman-Deurloo I-KK, Roos MA, Aluwini S. HDR monotherapy for prostate cancer: a simulation study to determine the effect of catheter displacement on target coverage and normal tissue irradiation. Radiother Oncol 2011;98:192–7. https://doi.org/10.1016/j.radonc.2010.12.009.
[30] Brock KK, Mutic S, McNutt TR, Li H, Kessler ML. Use of image registration and fusion algorithms and techniques in radiotherapy: Report of the AAPM Radiation Therapy Committee Task Group No. 132. Med Phys 2017;44:e43–76. https://doi.org/10.1002/mp.12256.
[31] Fitzpatrick JM. Detecting failure, assessing success. In: Hajnal J V., Hill DLG, Hawkes DJ, editors. Med. Image Regist., Washington: Biomedial Engineering Series; 2001, p. 117–36. https://doi.org/10.1201/9781420042474.ch6.
[32] McGeachy P, Watt E, Husain S, Martell K, Martinez P, Sawhney S, et al. MRI-TRUS registration methodology for TRUS-guided HDR prostate brachytherapy. J Appl Med Phys 2021;22:284–94. https://doi.org/10.1002/acm2.13292.